Radio-Optical Dual-Mode Communication Modules Integrated With Planar Antennas

Anatoliy O. Boryssenko, *Member, IEEE*, Jun Liao, *Member, IEEE*, Juan Zeng, *Member, IEEE*, Shengling Deng, *Member, IEEE*, Valencia M. Joyner, *Member, IEEE*, and Z. Rena Huang, *Member, IEEE*

***Abstract*—This paper presents new results on integrated devices for radio and free-space optical dual-mode communication. Two novel hybrid packaging schemes using two different microwave printed antenna designs are presented for the integration of radio-optical front-end circuits on a planar compact printed circuit board with shared electrical and structural components. Full-wave electromagnetic (EM) simulations are presented for antenna optimization to minimize EM interference between the radio and optical circuits. A hybrid radio-optical package design is developed, prototyped, and experimentally studied using a modified quasi-Yagi antenna with split directors to form pads for opto-electronic device integration. Dual-mode link connectivity is investigated in simulations and experiments. A data rate of 2.5 Gb/s is demonstrated for the optical channel despite 15–20-dB signal coupling between the optical and microwave circuits.**

***Index Terms*—Antenna, dual-mode wireless communication, integration, optical receiver, optical transmitter, packaging designs.**

I. Introduction

THERE IS an increasing interest in hybrid communication systems to combine the advantages of radio and optical free-space signaling for future communication and network technologies with increased bandwidth, reduced power consumption and cost, high adaptability to dynamic operational environment, and other promising features [1]–[3]. Dual-modality imaging incorporating microwave and optical sensors also represents a practical interest for biomedical studies including early breast cancer detection [4]. To reach such goals, new integration and packaging techniques must be advanced to account for several orders of dimensional discrepancy between antenna geometries, measured typically in millimeters at microwaves, and characteristic sub-millimeter dimensions of the active optical components. Several hybrid integration approaches were demonstrated to solve this challenging problem by employing single-module and single-chip designs [5]–[7].

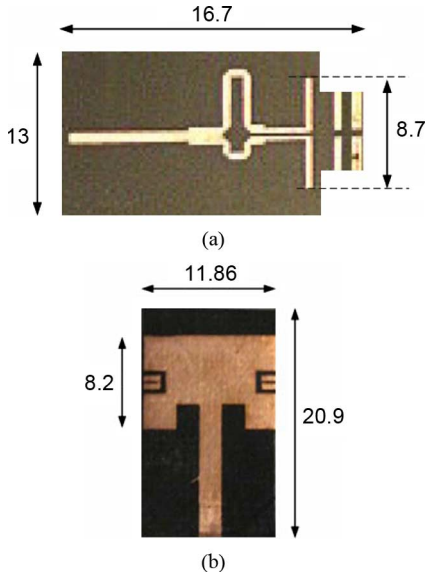

Fig. 1. Two printed antennas used for hybrid radio-optical packaging studies. (a) Quasi-Yagi. (b) Microstrip patch. All dimensions are in millimeters.

Here we report results of ongoing multiuniversity research efforts in the design, development, and testing of miniaturized radio-optical transceiver modules for combined radio-optical wireless communications. The research outcome will accelerate deployment of sensor networks by providing agile and reliable connectivity with long standby time and low manufacturing cost. Two hybrid radio-optical packaging schemes are considered, which are based on two versions of the microwave antennas: quasi-Yagi antenna [1], [8], [10] and microstrip patch antenna [9], as shown with their major dimensions in Fig. 1. These designs are tuned to operate around 11 GHz for a narrowband radio link and several gigabit per second data rates for an optical link. Both designs are developed by taking advantage of the dimensional difference between the microwave antenna and optical front-end elements. Specifically, the optical elements share some physical space with microwave circuits to minimize the overall packaging area/volume and align directions of optical and microwave radiation. Both designs with quasi-Yagi antenna [see Fig. 1(a)], and microstrip patch antenna [see Fig. 1(b)], are first analyzed in numerical simulations and then designed, prototyped, and experimentally tested.

Coupling from the microwave circuits to the optical transmitter and receiver front-ends is important in the view of

Manuscript received April 15, 2009; revised September 29, 2009. First published January 19, 2010; current version published February 12, 2010. This work was supported in part by the Rensselaer Polytechnic Institute under an Internal Seed Grant, by the National Science Foundation (NSF) under Grant ECCS-0823946, and by the Collaborative Biomedical Research (CBR) Program Grant, University of Massachusetts, Amherst.

A. O. Boryssenko is with the Department of Electrical and Computer Engineering, University of Massachusetts, Amherst, MA 01003 USA (e-mail:boryssen@ecs.umass.edu).

J. Liao, S. Deng, and Z. R. Huang are with the Department of Electrical, Computer and Systems Engineering, Rensselaer Polytechnic Institute, Troy, NY 12180 USA (e-mail: liaoj2@rpi.edu; dengs@rpi.edu; huangz3@rpi.edu).

J. Zeng and V. M. Joyner are with the Department of Electrical and Computer Engineering, Tufts University, Medford, MA 02155 USA (e-mail: juan.zeng@ece.tufts.edu; vjoyner@ece.tufts.edu).

Color versions of one or more of the figures in this paper are available online at http://ieeexplore.ieee.org.

Digital Object Identifier 10.1109/TMTT.2009.2038441

signal transmission integrity issues due to shared on-board space. Unlike optical modulators that are controlled by electric signals such as Mach–Zehnder modulators [14], the research described here is aiming to create a module to support two separate wireless channels: radio and optical free-space links. It is predictable that the electric signal/power is coupled into the optical subsystem because of packaging in a very tight space with shared structural components. This phenomenon is observed through numerical simulation, namely, commercial full-wave solvers including Ansoft High Frequency Structure Simulator (HFSS) and CST Microwave Studio. By careful design, as shown in this paper, the mutual coupling between the microwave and optical front-end circuits is minimized. It is especially lowered in the case of the microstrip patch assembly. The predicted impact of mutual coupling and link performance degradation are in a good agreement with measured results. The tested radio-optical modules demonstrate a data rate of 2.5 Gb/s in the duplex dual-channel communication configuration regardless of noticeable 15–20-dB coupling between radio and optical channels in the case of the quasi-Yagi antenna assembly.

The assembly and testing of optical elements with both the antennas are experimentally demonstrated. The discussion and comparative analysis of optical elements co-integrated with a microstrip patch antenna is built upon previous work presented in [1] and a comparison will be presented in this paper.

II. Radio-Optical Hybrid Modules With Quasi-Yagi Antenna

A quasi-Yagi antenna [see Fig. 1(a)] is first considered in this study for the hybrid radio-optical packaging because of the convenience in integration of two separate microwave and optical boards at the initial experimental phase [9]. The quasi-Yagi antenna board is printed on an RT/Duriod 6010 substrate with a thickness of 0.635 mm and relative permittivity of 10.2. This antenna is inherently reasonably broadband and exhibits high front-to-end ratio radiation along the antenna axis [7]. For the purpose of this study, the quasi-Yagi antenna design is modified by using split directors to provide options for packaging with both optical photodetectors (optical receiver) and laser diodes (optical transmitter). In addition, the antenna direction of the maximum radiation is altered from the original direction along the antenna axis to the direction that is normal to the antenna board to align the signal propagation directions of optical and microwave radiation. This beam alteration is achieved by backing the antenna board by a metal reflector (ground) at the bottom. This type of design adjustment exhibits a certain degradation of radiation performance [11], which is not critical for the proof-of-concept initial studies, while enabling faster prototyping and testing. In particular, the realized antenna gain of the modified quasi-Yagi is just 0.5 dBi against 4–5 dBi for the same antenna with regular radiation direction, as predicted in HFSS simulations.

The HFSS model of the antenna used for this study is shown in Fig. 2. In the model of this package, several optical ports are assigned between external tips of the split directors and the system ground at the board bottom [see Fig. 2(a)] of the quasi-Yagi antenna. Bondwires are used for the optical components placed on the pads (directors) to simulate signal return path with optical components added [see Fig. 2(b)]. Full-wave electromagnetic (EM) simulations using either HFSS or CST enables evaluation of the major electrical characteristics of this package, as illustrated in Fig. 3, for some representative component of the 5×5 terminal scattering matrix. The modified quasi-Yagi antenna demonstrates good matching to the feed line according to Fig. 3. This is achieved due to 50-Ω loads applied at the optical ports that, as expected, contribute to the lowering of antenna radiation efficiency from one side, but supports antenna matching on the opposite side at an acceptable level by compensating the effect of the bottom ground plane. This ground plane is used to alter the beam direction as above mentioned. Apparently, EM coupling appears in this layout because the same structural elements are shared as the antenna directors and optical circuit pads. The magnitude of computed coupling between the antenna port (#1) and, e.g., optical ports #2–3 is shown in Fig. 2(b) with respect to the 50-Ω reference impedance. Specifically, the coupling approaches 15–20 dB around the antenna resonance frequency around 11 GHz for the layouts in Fig. 2. This coupling seems negligible in the case of optical transmitters due to the large drive currents measured typically about 100 mA, but might exhibit a perceptible effect in the optical receiver, where weak photocurrent signals of a few μA are amplified, as further revealed.

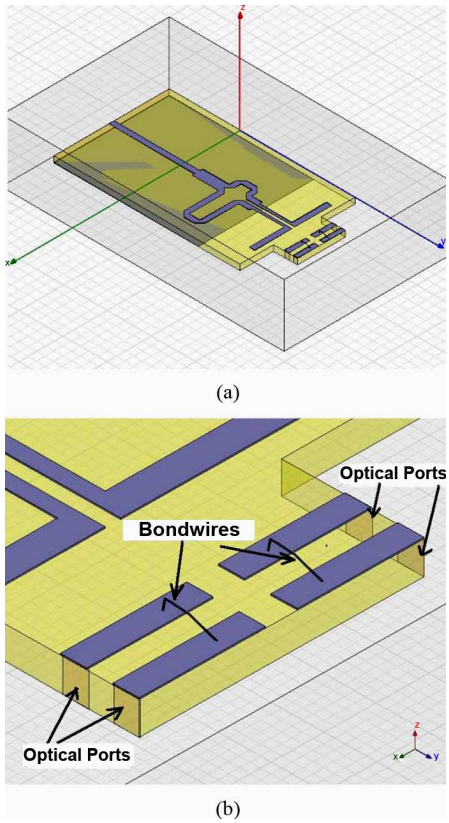

Fig. 2. HFSS computational model of the quasi-Yagi antenna with split directors used concurrently as pads to mount optical diodes. (a) Model overview. (b) Magnified portion highlighting connections to optical circuitry through four assigned optical ports to model mutual coupling between the antenna and optical ports (from [1]).

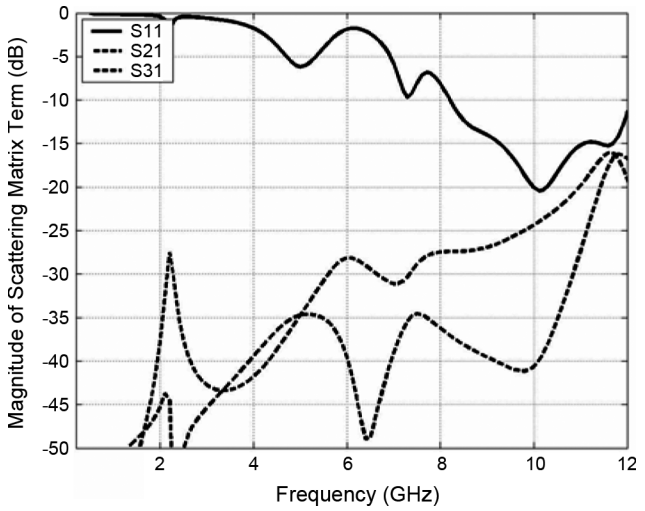

Fig. 3. HFSS predicted component of the 5×5 scattering matrix in decibels including return loss for the antenna port ($S11$) and coupling between the antenna port and two optical ports ($S21$ and $S31$) with slight asymmetry appearing due to difference in shape and position of the bondwires [see Fig. 2(b)]. Optical ports are terminated to 50 Ω.

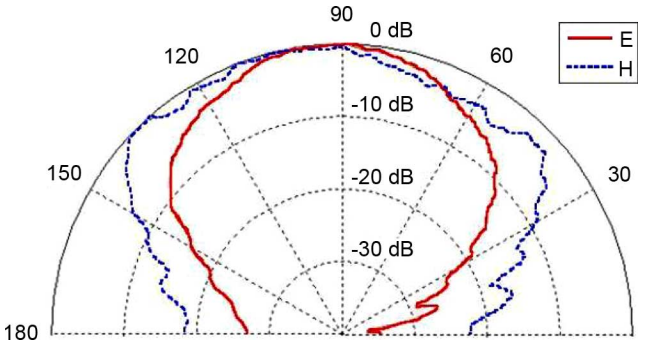

Fig. 4. Measured E- and H-plane antenna radiation patterns (90° reference direction corresponds to the Z-axis in Fig. 2).

The E- and H-plane sections of the antenna radiation pattern measured using the 1.5×1.5 m near-field NSI scanner are illustrated in Fig. 4, showing good antenna directivity.

III. Radio-Optical Hybrid Modules With Microstrip Patch Antenna

The microstrip patch antenna [see Fig. 1(b)] is analyzed in full-wave CST simulations [see Fig. 5(a)] as an alternative design solution with respect to the quasi-Yagi antenna to improve the electrical performance of the latter. In particular, the complete radio-optical design requires a single dielectric substrate and two layers of conductors on both faces of the substrate. Furthermore, this antenna structure conserves surface area for placement of all conductor traces and circuits for radio and optical transmission. In addition, a quasi-Yagi antenna is end-fire, while the laser diodes are surface emitters, thus there is an angle between the maximum radiation directions and the optical axes of the optical elements. The beam direction alteration leads to the antenna efficiency loss as demonstrated and it is avoided in the microstrip design. As a result of numerical studies, the optimized microstrip patch antenna structure [see Fig. 5(a)] occupies a small surface area of 2.54×2.54 cm^2. The optical circuits are represented by signal traces with dummy resistors to

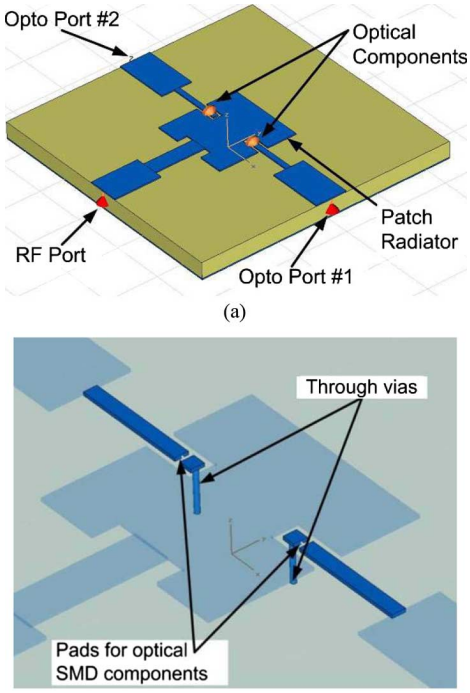

Fig. 5. CST models of the radio-optical assembly based on microstrip patch antenna. (a) 2.54×2.54 cm^2 substrate (Duroid: $t = 1.5$ mm, $\epsilon_r = 2.2$). (b) Magnified portion highlighting pads for optical component and return signal path formed through vias. The antenna is fed through the antenna radio port and two optical ports #1 and #2 provide connections to optical transmit/receive front-ends.

model the equivalent impedance of the optical components. To conserve area, the optical component pads are located in rectangular notches on opposite sides of the patch conductor. The mutual coupling is expected to be low because the lowest TEM resonance patch mode has a zero field in the area where the optical components will be placed [8]. The two optical ports, one for the transmitter and the other for the receiver, include two microstrip conductor sections. The optical return signal path is supported by the same bottom ground as for the microwave antenna by using the through vias [see Fig. 5(b)]. Using the same ground in a single layer for both radio and optical circuits enables less noise and interference. In a practical design, the dummy component of the optical circuits will be replaced by corresponding optical chips, as further shown in Section IV.

The scattering matrix of the radio-optical circuit layout in Fig. 5(b) is numerically predicted in CST simulations and illustrated in Fig. 6. The antenna can be matched to the required operational frequency, e.g., 11 GHz, with very low return loss while providing high realized gain in the range 6–7 dBi shown in the CST simulations. Mutual coupling is nearly 10 dB lower at the antenna resonance frequency compared to this feature of the quasi-Yagi antenna (Fig. 3) that eventually improves signal integrity for this design.

The simulated antenna radiation pattern at 11 GHz is shown in Fig. 7 and exhibits high realized gain and radiation efficiency. In particular, the predicted realized gain is about 6.5 dBi compared to just 0.5 dBi simulated for the quasi-Yagi antenna design (Fig. 2) with optical ports loaded in both cases with equivalent resistive loads to model the presence of optical components.

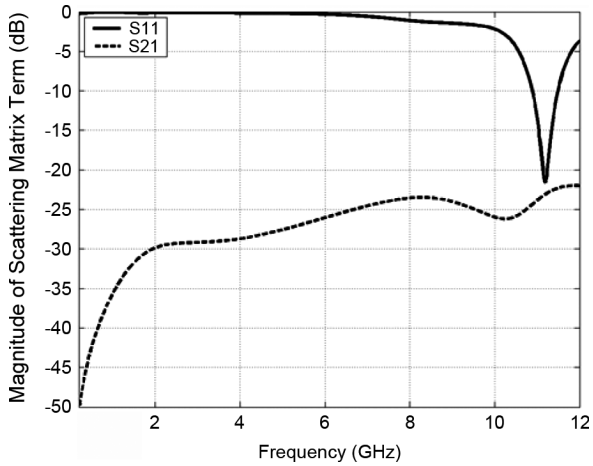

Fig. 6. CST predicted component of the 3×3 scattering matrix in decibels illustrated for return loss at the antenna port ($S11$) and coupling between the antenna port and an optical port ($S21$ and the same for $S31$ due to structural symmetry. Dummy 50-Ω resistors are used to mimic the effect of the optical components.

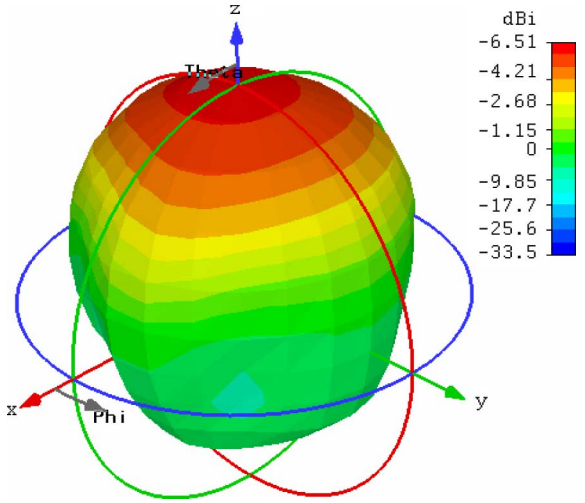

Fig. 7. CST predicted 3-D antenna radiation pattern of the patch antenna at 11 GHz normalized in terms of realized gain with total radiation efficiency of 95% using dummy 50-Ω resistors to simulate the presence of the optical components on pads in shared physical space.

IV. Prototypes of Radio-Optical Hybrid Transmit/Receive Modules

Both the design concepts are prototyped for experimental studies including the transmitter and receiver modules for the quasi-Yagi antenna [see Fig. 1(a)] and the receiver module for the microstrip patch antennas [see Fig. 1(b)]. A rationale to consider only the receiver in the second antenna case relies on the fact that the mutual coupling between the optical and radio front-ends affects the hybrid receivers without a notable impact on the hybrid transmitters, as demonstrated in Section VI.

A. Transmitter and Receiver Hybrid Modules With Quasi-Yagi Antenna

The radio-optical dual mode transmitter and receiver modules with the quasi-Yagi antenna are built on a four-layer FR4 printed circuit board (PCB) and shown in Fig. 8. For free-space optical processing, the use of vertical-cavity surface-emitting

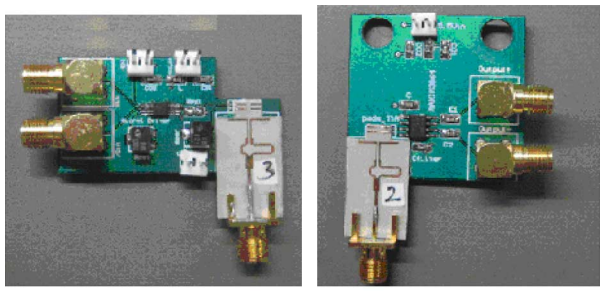

(a) (b)

Fig. 8. Photographs of fabricated radio-optical modules packaged with the quasi-Yagi antenna. (a) Transmitter. (b) Receiver (from [1]).

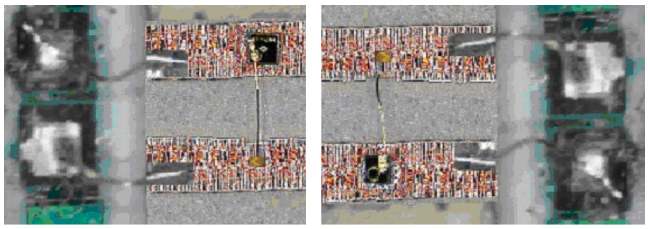

(a) (b)

Fig. 9. Photographs of details to mount the optical die components on the pads shared with the quasi-Yagi antenna. (a) VCSEL on the antenna pad to construct a transmitting radio-optical. (b) p-i-n on the antenna pad to construct the receiver board on PCB (from [1]).

laser (VCSEL) and p-i-n diode devices is attractive for future low-cost hybrid/flip-chip packaging with active silicon complementary metal–oxide semiconductor (CMOS) electronic circuits [12], [13]. CMOS technology enables high levels of integration combining sensitive front-end circuits with digital processing circuits on the same die. For this preliminary study, hybrid integration is achieved by wirebonding bare die opto-electronic devices to commercial optical transmitter and receiver circuits. On the transmitter board, a commercial high-speed current switch laser diode driver (Micrel SY88922V) is employed to drive a bare die VCSEL (Optowell SM85-2N001). The VCSEL is attached to the director of the transmitting quasi-Yagi antenna. On the receiver board, a high-speed transimpedance amplifier chip (MAX3864) is mounted to amplify the single-ended photocurrent signal from a p-i-n diode (Optowell SP85-3N001). The p-i-n is assembled to the director of the receiving quasi-Yagi antenna.

The VCSEL on the transmitter board is fabricated on a gallium–arsenide (GaAs) substrate with a peak emission of 2.5 mW at $\lambda = 850$ nm. The die size of the VCSEL is 300×300 μm^2. The GaAs p-i-n on the receiver board has a responsivity of 0.6 A/W. The die size of the p-i-n is 250×250 μm^2. The N contacts of both the VCSEL and the p-i-n are attached to antenna director pads by conductive epoxy adhesives (Resinlab SEC 1233). The P contacts of the VCSEL and p-i-n are wirebonded to the remaining antenna director using gold wires with a diameter of 25 μm. The antenna director pads are electrically connected to the PCB bonding pads with silver-coated copper wires. The length of the bonding wires are minimized to reduce ringing and peaking induced by the parasitic capacitance and inductance. Details of the optical devices packaged on the antenna director pads are shown in Fig. 9.

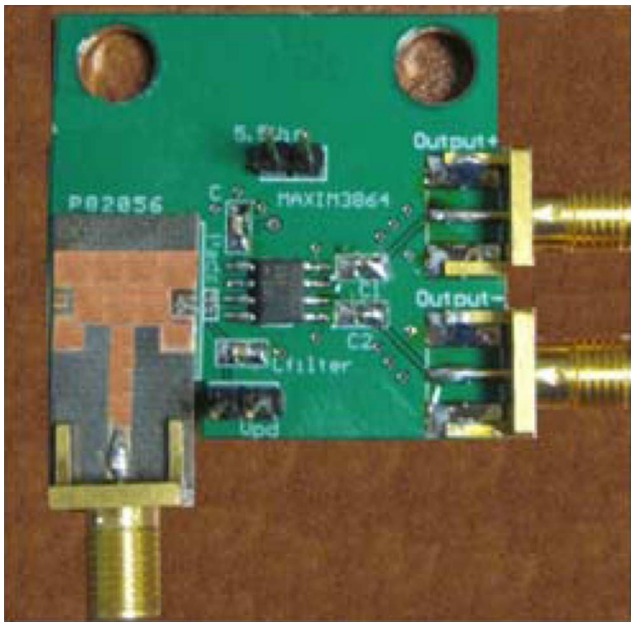

Fig. 10. Photographs of fabricated radio-optical receiver module packaged with the microstrip patch antenna [see Fig. 1(b)].

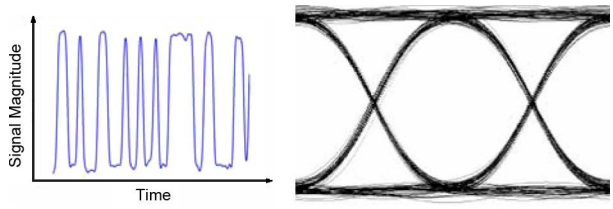

Fig. 11. MATLAB model simulation for weak coupling between the microwave and optical front-ends. (a) Portion of the transmitted $2^7 - 1$ test PRBS mixed with random phase 10-GHz time–harmonic signal. (b) Computed eye diagram.

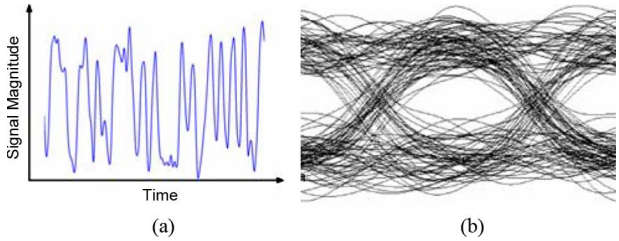

Fig. 12. MATLAB model simulation for strong coupling between the microwave and optical front-ends. (a) Portion of the transmitted $2^7 - 1$ test PRBS mixed with random phase 10-GHz time–harmonic signal. (b) Computed eye diagram.

B. Receiver Module With Microstrip Patch Antenna

The radio-optical dual mode receiver prototype with the microstrip patch antenna is shown in Fig. 10. The assembly consists of the two superimposed boards for quick prototyping similarly to the approach implemented in Fig. 8. Specifically, the optical circuit board is very similar to the board used with the quasi-Yagi antenna [see Fig. 8(b)]. This optical board is also built on a four-layer FR4 PCB using essentially the same electronic components, as indicated above. Both of the boards also have comparable outer dimensions. The microstrip patch antenna board [see Fig. 1(b)] is printed on the RT/Duroid 5880 substrate of dialectical permittivity 2.2 and thickness of 0.8 mm. It is observed that some area conservation is achieved in the receiver design in Fig. 10 compared to the receiver in Fig. 8(b) because of the compact geometry of the microstrip patch antenna.

Note that the actual optical front-end in the receiver prototype shown in Fig. 10 is based on a differential network unlike the simplified unbalanced network used in the simulated design in Fig. 5. This fact does not change mutual coupling between the optical and microwave front-end circuits, but enables integration with the differential inputs of the MAX3864 transimpedance amplifier chip. In the case of the board in Fig. 10, the same p-i-n chips and its assembling technology is employed as described above for the board in Fig. 8(b).

V. ANALYSIS OF LINK PERFORMANCE UNDER IMPACT OF COUPLING BETWEEN MICROWAVE AND OPTICAL CIRCUITS

The bit error rate (BER) performance of the optical link is directly determined by the noise performance of the optical receiver circuit, according to the following expression:

$$E = Q\left(\frac{P_{\rm rec} \cdot R_{ph}}{I_{n,\rm rms}}\right) \tag{1}$$

where E is the BER factor, $P_{\rm rec}$ is the average received optical power, and $Q(\cdot)$ is the Q function and can be approximated with high accuracy by

$$Q(x) \approx \frac{1}{x\sqrt{2\pi}} \exp\left(-\frac{x^2}{2}\right), \qquad x > 3 \tag{2}$$

and R_{ph} is the detector responsivity in A/W. The square root of the input-referred noise-current spectral density integrated over the receiver's noise equivalent bandwidth (Δf) yields the total mean-square input-referred noise current $I_{n,\rm rms}$

$$I_{n,\rm rms} = \sqrt{\overline{I_n^2} \cdot \Delta f}. \tag{3}$$

Thus, mutual coupling between the microwave and opto-electronic front-end circuits will affect the optical link by noise coupling at opto-to-electronic interface. The BER performance will be adversely affected by two noise mechanisms, which are: 1) laser driver current noise corrupting $P_{\rm rec}$ and 2) input current noise at the optical receiver front-end increasing $I_{n,\rm rms}$.

The eye pattern can be predicted based on the simulated data in Figs. 3 and 6, respectively, for the quasi-Yagi antenna and the microstrip patch antenna using a simple MATLAB model. In this model, reception of the $2^7 - 1$ pseudorandom bit sequence (PRBS) optical signal transmitted at a 2.5-Gb/s rate is considered. Additionally, a time–harmonic signal at 11 GHz is mixed with the PRBS signal as a noise component with magnitude corresponding to the predicted magnitudes of the inter-channel coupling and random phase because the optical and radio signals are not locked in phase. For illustrations, two channel conditions are treated for low $(-25$ dB$)$ and high $(-15$ dB$)$ coupling between the optical and microwave front-end circuits. Respective portions of the transmitted $2^7 - 1$ PRBS are plotted in Figs. 11(a) and 12(a), while the respective eye diagrams are shown in Figs. 11(b) and 12(b). Note that the simulated data

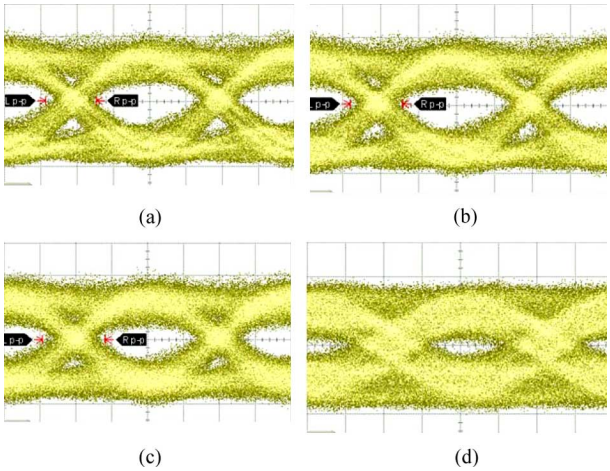

Fig. 13. Measured 2.5-Gb/s eye pattern for receiver prototype board with the quasi-Yagi antenna [see Fig. 8(b)] for the microwave antenna port fed with different power levels. (a) No microwave signal. (b) 0 dBm. (c) 7 dBm. (d) 14 dBm. The time scale is 100 ps/div and magnitude scale is 9.6 mV/div.

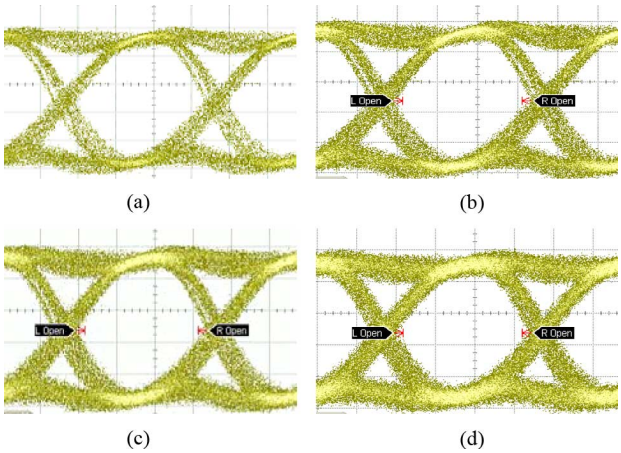

Fig. 14. Measured 2.5-Gb/s eye pattern for the receiver prototype board with the microstrip patch antenna [see Fig. 10] for the microwave antenna port fed with different power levels. (a) No microwave signal. (b) 0 dBm. (c) 7 dBm. (d) 14 dBm. The time scale is 100 ps/div and magnitude scale is 20 mV/div.

eye diagram is in a good agreement with measured results under identical conditions and bit rate for the radio-optical receiver, as further shown in Figs. 13 and 14.

VI. Experimental Studies of Hybrid Receiver and Transmitter Prototypes

A set of tests are carried out to assess the impact of the mutual radio-optical coupling in the prototyped hybrid boards in Figs. 8 and 10 by measuring the eye pattern of the optical receiver as the microwave antennas are fed for different input power levels. In particular, the tests are performed for: 1) the hybrid receiver board with the quasi-Yagi antenna [see Fig. 8(b)]; 2) the hybrid receiver board with the microstrip antenna (see Fig. 10); and 3) hybrid transmitter board with the quasi-Yagi antenna [see Fig. 8(a)]. In the receiver cases, the data pattern input to the optical laser driver circuit is 2.5-Gb/s PRBS, similar to the MATLAB link model in Section V.

A. Hybrid Receiver Prototype With Quasi-Yagi Antenna

In this prototype board [see Fig. 8(b)], the antenna induced current is coupled into the optical channel through the bondwire connecting the optical photodetector to the front-end transimpedance amplifier circuit. As the antenna input power increases, the EM induced current is higher and more noise is coupled into the optical channel, which dramatically degrades the signal-to-noise ratio. The corresponding measured eye diagrams are shown in Fig. 13. As shown in Fig. 13(d), the eye is almost closed when the antenna is fed with 14-dBm power. In general, the measured diagrams are qualitatively similar to the corresponding predicted patterns in the MATLAB model. Specifically, this similarity is respectively observed between the simulated data in Figs. 11(b) and 12(b) from one side, and the measured data in Figs. 13(a) and 13(d) from the other side.

However, it is worth noting that for indoor wireless communication, the power fed into the transmission antenna is much lower than 14 dBm. Furthermore, in the presented study, the microwave antenna integrated with a p-i-n diode operates in the receiving mode, which will minimize the microwave noise coupling to the photoreceiver. The phenomenon appearing in Fig. 13(d) accounts for the worst case in terms of radio-optical coupling. For real applications, Fig. 13(a) and (b) is sufficient to study the coupling between the two links.

B. Hybrid Receiver Prototype With Microstrip Patch Antenna

The board with the microstrip patch antenna (Fig. 10) is similarly tested as the above case with the Yagi antenna by varying the input microwave power at the antenna port at the same gradual levels. The measured eye diagrams are shown in Fig. 14. Unlike the case in Fig. 13, the derived results for this prototype board do not exhibit a notable impact of the microwave signals on the optical channel. Essentially, the experimental eye diagrams for this case are somewhat analogous to the simulated case in MATLAB for low mutual coupling between the microwave and optical front-ends shown in Fig. 11(b). Thus, the derived results confirm the theoretical prediction that follows from comparison of the simulated dependencies in Figs. 3 and 6. In fact, the receiver board with the microstrip antenna looks much robust with respect to the mutual coupling effects compared to the board based on the quasi-Yagi antenna.

C. Hybrid Transmitter Prototype With Quasi-Yagi Antenna

To evaluate the feasibility of high data-rate optical communication under the impact of inter-channel mutual coupling, the eye diagram of an optical link is tested. The link consists of the radio-optical transmitter [see Fig. 8(a)], receiver [see Fig. 8(b)], and lens alignment system. The data pattern input to the optical laser driver remains as a 2.5 Gb/s, $2^7 - 1$ PRBS. In this setup, the microwave signal is fed into the antenna on the transmitter board, while the antenna on the receiver board is connected to a spectrum analyzer to measure the received microwave power. When the transmission antenna is fed with a 14-dBm radio signal at 10 GHz, the received microwave power is -14 dBm. The measured optical link eye pattern under the condition of a nonradiating antenna is shown in Fig. 15(a). Fig. 15(b) displays the eye pattern when the microwave power is delivered

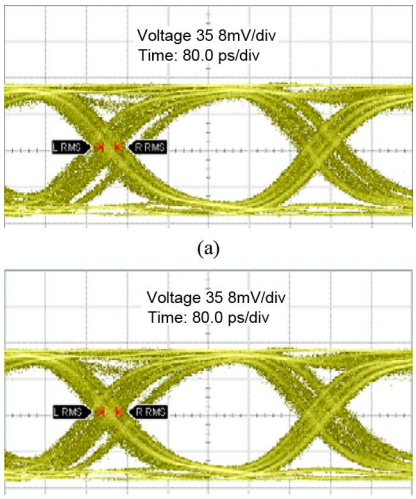

Fig. 15. Measured eye pattern for optical link when the quasi-Yagi antenna is: (a) turned off and (b) turned on.

to the antenna. As previously discussed, the antenna power leakage in the optical front-end circuits has little effect on the transmitter side and can be neglected on the receiver side if the radio receiving power is low. Therefore, the coupling from the radio channel to optical channel is negligible in this setup and no noticeable change in the eye diagram is observed when the antenna is on or off, validating the theoretical prediction.

VII. Conclusion

Two novel hybrid radio-optical transceiver configurations with different microwave antenna structures are first studied numerically in full-wave HFSS and CST simulations. A set of transmitter and receiver modules for two different microwave printed antennas is developed and implemented in several packaged modules prototyped for an experimental dual-mode radio-optical communication system. Being tested, the new packaging approach reveals that it is feasible to design radio and optical circuits with shared structural components and physical space to tackle dimensional discrepancies between radio and optical devices.

In our studies of the packaging design with the quasi-Yagi antenna (Fig. 8), the metal director pads of a planar antenna are used as the mounting pads for optical semiconductor elements, resulting in an ultra-compact hybrid radio-optical package design through the shared areas of the radio and optical transmitter and receivers. Shared electrical interconnections between radio and optical circuit components introduce additional interference signals due to EM coupling. Our analysis also shows that the microwave induced noise is negligible for the transmitter, but might degrade the signal integrity and BER performance of the optical receiver. Experimentally, a dual-mode radio-optical transmitter and receiver pair was demonstrated with an optical transmission rate of 2.5 Gb/s.

In our studies of the packaged receiver prototype with the microstrip patch antenna, a different robust scheme is implemented and successfully tested. In particular, the packaged prototype (Fig. 10) occupies less physical space compared to the prototype in Fig. 8(b). It also exhibits notably lower signal integrity degradation because of lower coupling between the microwave and optical front-ends.

Our ongoing studies are focused on several other perspective integrated radio-optical packaging designs to minimize signal integrity degradation, approach to single-chip solutions, and exploit other types of EM radiators. Our future developments will be focused on providing the same or comparable data throughput for both radio and optical link modalities by exploiting a suitable UWB antenna and signaling scheme.

References

[1] A. O. Boryssenko, J. Liao, J. Zeng, V. Joyner, and Z. R. Huang, "Studies on RF-optical dual mode wireless communication modules," in *IEEE MTT-S Int. Microw. Symp. Dig.*, Jun. 2009, pp. 805–809.

[2] S. D. Milner and C. C. Davis, "Hybrid free space optical/RF networks for tactical operations," in *Proc. IEEE Military Commun. Conf.*, Nov. 2004, vol. 1, pp. 409–415.

[3] S. Deng, J. Liao, Z. H. Rena, M. Hella, and K. Connor, "Wireless connections of sensor network using RF and free space optical links," *Proc. SPIE*, vol. 6773, pp. 677307.1–677307.11, 2007.

[4] , K. D. Paulsen, P. M. Meaney, and L. Gilman, Eds., *Alternative Breast Imaging: Four Model-Based Approaches*. New York: Springer, 2005.

[5] J. J. Lin, L. Gao, A. Sugavanam, X. Guo, R. Li, J. E. Brewer, and K. O. Kenneth, "Integrated antennas on silicon substrates for communication over free space," *IEEE Electron Device Lett.*, vol. 25, no. 4, pp. 196–198, Apr. 2004.

[6] F. Touati and M. Pons, "On-chip integration of dipole antenna and VCO using standard BiCMOS technology for 10 GHz applications," in *Proc. IEEE Eur. Solid-State Circuits Conf.*, Sep. 2003, pp. 493–496.

[7] B. W. Cook, S. Lanzisera, and K. S. J. Pister, "SoC issues for RF smart dust," *Proc. IEEE*, vol. 94, no. 6, pp. 1177–1196, Jun. 2006.

[8] W. R. Deal, N. Kaneda, J. Sor, Y. Qian, and T. Itoh, "A new quasi-Yagi antenna for planar active antenna arrays," *IEEE Trans. Microw. Theory Tech.*, vol. 48, no. 6, pp. 910–918, Jun. 2000.

[9] R. Bancroft, *Microstrip and Printed Antenna Design*. Raleigh, NC: SciTech Publishing, 2008.

[10] J. Liao, S. Deng, F. Smith, Z. R. Huang, and K. A. Connor, "Integrated laser diodes and photodetectors with antenna for dual-mode wireless communication," in *Proc. IEEE LEOS Annu. Meeting*, Oct. 2007, pp. 264–265.

[11] S. E. Melais and T. M. Weller, "A quasi Yagi antenna backed by a metal reflector," *IEEE Trans. Antennas Propag.*, vol. 56, no. 12, pp. 3868–3872, Dec. 2008.

[12] C. L. Schow, F. E. Doany, C. Chen, A. V. Rylyakov, C. W. Baks, D. M. Kuchta, R. A. John, and J. A. Kash, "Low-power 16×10 Gb/s bi-directional single chip CMOS optical transceivers operating at $\ll 5$ mW/Gb/s/link," *IEEE J. Solid-State Circuits*, vol. 44, no. 1, pp. 301–313, Jan. 2009.

[13] R. Pu, C. Duan, and C. W. Wilmsen, "Hybrid integration of VCSEL's to CMOS integrated circuits," *IEEE J. Sel. Topics Quantum Electron.*, vol. 5, no. 2, pp. 201–208, Mar./Apr. 1999.

[14] R. Becker, "Broad-band guided-wave electrooptic modulators," *IEEE J. Quantum Electron.*, vol. 20, no. 7, pp. 723–727, Jul. 1984.

Anatoliy O. Boryssenko (M'98) received the M.Sc. E.E. and Ph.D. E.E. degrees from the Kiev Polytechnic Institute, Kiev, Ukraine.

He was an Associate Professor with the Kiev Polytechnic Institute and a Research and Development Engineer with companies related to millimeter-wave and UWB communication and sensor systems. Since 2000, he has been with the University of Massachusetts, Amherst, where he is currently a Research Associate Professor with the Department of Electrical and Computer Engineering. His research interests include subsurface radar imaging, broadband and UWB antenna and array design, applied and computational electromagnetics, and signal processing and system design for radar, sensing and imaging.

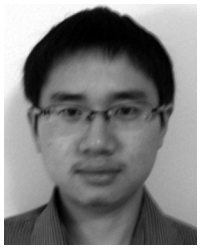

Jun Liao (M'07) received the B.S. degree from the Beijing University of Posts and Telecommunications, Beijing, China, in 2006, and is currently working toward the Ph.D. degree in electrical, computer and systems engineering at the Rensselaer Polytechnic Institute, Troy, NY.

His research interest includes RF/opto hybrid packing, planar antenna design, and free-space optical communication.

Juan Zeng (M'03) received the B.S. degree in electronic science and technology from the Harbin Institute of Technology (HIT), Harbin, China in 2007, and is currently working toward the M.S. degree in electrical engineering at Tufts University, Medford, MA.

Her research interests include CMOS circuits for broadband wireless applications.

Ms. Zeng was the recipient of the MediaTek Inc. and Wu Ta-You Scholar Award presented by the Harbin Institute of Technology in 2006 and the Dean's Fellowship presented by Tufts University in 2007.

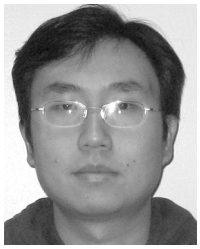

Shengling Deng (M'08) received the B.S. in physics from Nanjing University, Nanjing, China in 2002, the M.S. in electrical engineering from the University of Florida, Gainesville, in 2005, and is currently working toward the Ph.D. degree at the Rensselaer Polytechnic Institute, Troy, NY.

His research interest includes III–V metal–semiconductor–metal (MSM) integration, Si-based electrooptic (EO) modulators, and integrated optics on silicon-on-insulator (SOI).

Valencia M. Joyner (M'98) received the S.B. and M.Eng. degrees in electrical engineering and computer science from the Massachusetts Institute of Technology, Cambridge, in 1998 and 1999, respectively, and the Ph.D. degree from the University of Cambridge, Cambridge, U.K., in 2003.

She is currently an Assistant Professor with Tufts University, Medford, MA, where she leads the Advanced Integrated Circuits and Systems Group. Her current research interests include opto-electronic integrated circuit design for high-speed optical and RF wireless networks and biomedical imaging applications.

Dr. Joyner was the recipient of a Marshall Scholarship and National Science Foundation (NSF) Graduate Research Fellowship.

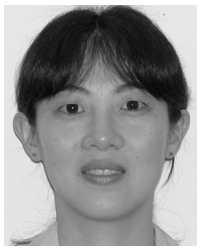

Z. Rena Huang (M'99) received the B.S. degree from the Beijing Institute of Technology, Beijing, China, in 1995, and the M.Sc. and Ph.D. degrees from the Georgia Institute of Technology, Atlanta, in 1999 and 2003, respectively.

She is currently an Assistant Professor with the Rensselaer Polytechnic Institute, Troy, NY. Her current research focus includes RF/opto packaging for high-speed low-power wireless communication, and integrated photonics for next-generation lightwave technology.